TÜBİTAK

Turkish Journal of Physics

http://journals.tubitak.gov.tr/physics/

Research Article

Turk J Phys
(2019) 43: 156 – 166

doi:10.3906/fiz-1809-12

Higher-order differential cross section calculation for the associated production of a W boson and jets in the electron decay channel at a center-of-mass energy of 13 TeV in proton-proton collisions

Kadir ÖCALAN*
Department of Aviation Management, Faculty of Aviation and Space Sciences, Necmettin Erbakan University, Konya, Turkey

Received: 15.09.2018 • **Accepted/Published Online:** 13.02.2019 • **Final Version:** 08.04.2019

Abstract: Higher-order cross sections for the production of a W boson in association with jets in the electron decay channel are presented in this study. Cross sections were calculated in a fully differential way using a computational framework based on proton-proton collisions at a center-of-mass energy of 13 TeV. The differential cross section predictions in the fiducial phase-space were compared at next-to-leading order (NLO) and next-to-NLO (NNLO) in perturbative quantum chromodynamics (pQCD). The differential results are reported for the variables including the jet multiplicity, the invariant mass of the W boson, transverse momentum, the jet rapidity, and the electron pseudorapidity that are sensitive to higher-order corrections in pQCD. The presented differential cross sections were generally improved in precision in the NNLO calculation. The total cross sections at NLO and NNLO are also reported in the fiducial phase-space. More accurate results were obtained in the calculation of the total production rates at NNLO. The results in all the calculations are given in the W^+ and the W^- boson decay channels separately to better assess the impact of the inclusion of higher-order corrections in those processes.

Key words: Standard model physics, quantum chromodynamics, W boson+jets, differential cross section calculations, total fiducial cross section calculations, NLO and NNLO precise calculations

1. Introduction

The associated production of a vector boson and jets at hadron colliders is a prominent process enabling precision tests of the standard model (SM). The productions of a weak vector boson (W or Z boson) in lepton decay channels and associated jets have large production rates and clean experimental signatures in proton-proton (pp) collisions at the CERN Large Hadron Collider (LHC). These processes can be used to provide precise tests for higher-order perturbative quantum chromodynamics (pQCD) calculations and substantial inputs for constraining parton distribution functions (PDFs) in the proton. Moreover, these processes constitute a major background in Higgs boson production and other SM processes such as single top quark and top quark pair productions. Their precise descriptions are not only a benchmark for the SM-related studies but also important for the new-physics searches such as supersymmetry and dark matter. The LHC experiments have acquired a large amount of pp collision data that can be used to tune descriptions of these processes in theoretical predictions. The predictions including next-to-leading order (NLO) and next-to-NLO (NNLO) corrections in pQCD can be improved to accurately describe experimental data using such processes.

*Correspondence: kadir.ocalan@konya.edu.tr

W boson production in association with jets (W+jets) has been characterized by the differential measurements of cross sections at the LHC as functions of several kinematical and angular observables that are reconstructed using the W boson and its leptonic decay products as well as the associated hadronic jets. The differential cross sections for W+jets have been measured by the CMS Collaboration using data collected at center-of-mass energies of 7 TeV [1] and 8 TeV [2]. The differential cross sections for W+jets have also been measured by the ATLAS Collaboration at 7 TeV [3] and 8 TeV [4] as well as by the LHCb Collaboration in the forward region of pp collisions at 8 TeV [5]. The CMS Collaboration has measured the W+jets differential cross sections at 13 TeV [6] for a broad range of variables including angular correlations between the muon and jets to probe into the contributions of real W boson emission from an energetic jet, which was studied by the ATLAS Collaboration with 8 TeV data [7]. In all of these complementary measurements, experimental data have been compared with predictions from various Monte Carlo event generators and higher-order QCD calculations comprising either NLO or NNLO corrections.

Precise calculations of the SM processes including W+jets production require the inclusion of QCD radiative corrections at the NLO and NNLO. The field of NNLO QCD computations has been rapidly evolving to provide fully differential calculations for various hadron collider processes. NNLO differential calculations based on the N-jettiness subtraction method have been available for quite some time for the Z boson production in association with inclusive one jet [8] and the W boson production in association with inclusive one jet [9, 10] processes. Despite the notable progress, publicly available NNLO computations typically employ a limited set of methods for the evaluation of the NNLO terms in their differential cross section calculations.

In this paper, a new computational framework MATRIX [11, 12] was used. MATRIX has the capability to allow application of realistic fiducial cuts on the phase-space of the respective leptonic final states to obtain fully differential cross sections up to NNLO in QCD for W+jets production. The (N)NLO calculation in MATRIX was achieved by using a process independent implementation of the transverse momentum q_T-subtraction method [13, 14] with a fully automated implementation of the Catani–Seymour dipole subtraction method [15, 16]. In MATRIX computations for W+jets production, all tree-level and one-loop amplitudes were acquired by using OPENLOOPS Monte Carlo program [17–20]. The leptonic decay channels provide clean experimental signatures with relatively lower background in comparison to semi-leptonic and hadronic decay modes of the W boson production at hadron colliders. The electron decay channel of the W+jets production is used only in this paper. The muon decay channel was not used anticipating that the level of precision to be achieved in the muon decay channel will be similar to that of the electron decay channel.

2. (N)NLO computations

In a computation of a QCD cross section at NNLO, tree-level contributions with up to two additional partons, one-loop contributions with one parton, and purely virtual contributions are required to be evaluated properly. The scattering amplitudes corresponding to such contributions in a complete NNLO calculation must be implemented by taking into account the presence of infrared (IR) divergences at intermediate stages of the calculation. The q_T-subtraction method [13, 14], where q_T refers to transverse momentum of colorless system (i.e. a system composed of particles without QCD interactions) in this formalism, is used to handle and cancel IR divergences in the MATRIX NNLO computation. In the q_T-subtraction method, the cross section σ for a process $pp \to F + X$, where F is a colorless system, can be written at NNLO as

$$d\sigma^F_{NNLO} = [d\sigma^{F+jet}_{NLO} - d\sigma^{CT}_{NNLO}] + H^F_{NNLO} \otimes d\sigma^F_{LO}. \tag{2.1}$$

In Eq. (2.1), the term $d\sigma_{NLO}^{F+jet}$ represents the cross section for the system $F+jet$ at NLO, while the process-independent counterterm $d\sigma_{NNLO}^{CT}$ guarantees the cancellation of the $F+jet$ cross section divergence at NNLO. The calculation is completed with the addition of the product term of the hard-collinear coefficient H_{NNLO}^{F} at NNLO [21] and the LO cross section $d\sigma_{LO}^{F}$ of the system F.

The contribution in the square bracket in Eq. (2.1) is formally finite in the limit $q_T \to 0$, but the terms $d\sigma_{NLO}^{F+jet}$ and $d\sigma_{NNLO}^{CT}$ are separately divergent. In the NNLO calculations employing the q_T-subtraction method, a residual dependence parameter $r = q_T/m$ is used, where m is the invariant mass of the colorless system. This residual dependence is due to power-suppressed terms that remain after the subtraction of the IR singular contribution at finite values and vanish only in the limit $q_T \to 0$. Furthermore, a cut-off value for this residual dependence r_{cut} is introduced to render both terms separately finite. In the differential cross section calculations of this paper at NNLO, $r_{cut} = 0.0015$ (0.15%) was used and below this cut $d\sigma_{NLO}^{F+jet}$ and $d\sigma_{NNLO}^{CT}$ terms were assumed to be identical up to power-suppressed contributions. The total cross sections in this paper are reported both for $r_{cut} = 0.15\%$ and for the extrapolation in the limit $r_{cut} \to 0$.

The MATRIX framework provides also computations for SM processes at NLO accuracy by including both QCD and electroweak (EW) corrections. The Catani–Seymour dipole subtraction method [15, 16] was used to perform the calculation of massless and massive partons at NLO. In the Catani–Seymour dipole subtraction method, a subtraction (addition) term is included in the calculation to cancel individual divergences of the real and virtual terms in the simplest form as

$$\sigma_{NLO} = \int_{m+1} d\sigma_R + \int_m d\sigma_V = \int_{m+1} [(d\sigma_R)_{\epsilon\to 0} - (d\sigma_A)_{\epsilon\to 0}] + \int_m [d\sigma_V + \int_1 d\sigma_A]_{\epsilon\to 0}. \tag{2.2}$$

In Eq. (2.2), $d\sigma_R$ ($d\sigma_V$) corresponds to the cross section of real emission contribution (virtual contribution) and is integrated for amplitude with m+1 (m) partons. Both $d\sigma_R$ and $d\sigma_V$ terms are separately IR divergent. The subtraction (addition) term $d\sigma_A$ which regularizes the divergences is integrated over m+1 parton phase-space. The $d\sigma_A$ term acts as a counterterm for $d\sigma_R$ and the integration of the first term on the right-hand side of the Eq. (2.2) can be carried out numerically for the limit ϵ pole $\to 0$. The integration of $d\sigma_A$ term in the second term on the right-hand side of the Eq. (2.2) can be carried out analytically over one parton phase-space leading to the ϵ poles. These poles can be combined with those in $d\sigma_V$ to cancel all the divergences in the limit $\epsilon \to 0$ and then the remaining integration over m parton phase-space can be carried out numerically.

3. Process settings and fiducial selections

The general setting for the cross section calculation of the W+jets production was based on pp collisions at the LHC using a center-of-mass energy of 13 TeV. The W+jets process in the electron decay channel $pp \to W + X \to e\nu_e + X$, where the W boson is indeed off-shell, was set up with the MATRIX framework. The W+jets process was split into $W^+ + X \to e^+\nu_e + X$ and $W^- + X \to e^-\bar{\nu}_e + X$ productions to figure out dependency of production rates on the polarization of the W boson. The final state X refers to at most one (two) additional parton(s) in the (N)NLO computation. Moreover, the renormalization scale μ_R and the factorization scale μ_F were both evaluated to be the W boson mass $\mu_R = \mu_F = 80.385$ GeV in the cross section computations. The scales were used to estimate uncertainties from missing higher-order contributions in the usual way by independently varying the μ_R and μ_F by a factor of 0.5 and 2. All possible combinations were

used in the variations with the exclusion of the cases where one scale was varied by a factor of 0.5 and the other one by a factor of 2 at the same time.

The *LHAPDF 6.2.0* [22] was used for the evaluation of PDFs from data files in the computations. The PDF sets *NNPDF30_lo_as_0118*, *NNPDF30_nlo_as_0118*, and *NNPDF30_nnlo_as_0118* were used from the NNPDF Collaboration [23] for the LO, NLO, and NNLO cross section calculations, respectively. The PDF sets were all based on a constant strong coupling $\alpha_s(m_Z) = 0.118$ assuming an EW scale specified by the Z boson mass.

The cross sections were calculated by considering realistic fiducial cuts on the phase-space that have been used in experimental results of the LHC. The lepton (i.e. either an electron or an anti-electron) was required to have transverse momentum $p_T > 25$ GeV in the pseudorapidity acceptance region of $|\eta| < 2.4$. The jets were clustered using the anti-k_T algorithm [24] with the distance parameter $\Delta R = 0.4$, where ΔR is defined using the separation in jet η and in jet azimuthal angle ϕ as $\Delta R = \sqrt{\Delta\eta^2 + \Delta\phi^2}$. The fiducial selection of the jets include $p_T > 25$ GeV requirement in the rapidity acceptance region of $|y| < 2.4$. The jets were selected to refer to all parton-level jets; gluons and 5 light quarks including a massless bottom quark b such as from the gluon splitting process $g \to b\bar{b}$, which is essentially needed to keep jet observables IR safe. A requirement is imposed for the final state neutrinos comprising electron-neutrinos and antielectron-neutrinos, such that p_T of sum of all neutrinos (so-called missing transverse momentum that is connected to detector-escaping property of neutrinos in an experiment) was required to be $p_T^{miss} > 20$ GeV. To this end, a fiducial cut was not specified for the invariant mass of the W boson such that $m_T(W) > 0$ GeV was used, where it can be expressed using the $\vec{p}_T(e)$, $\vec{p}_T^{miss}$, and $\Delta\phi$ in the directions of these vectors as $m_T(W) = \sqrt{2p_T(e)p_T^{miss}(1 - cos\Delta\phi)}$. The $m_T(W)$ selection makes sense for experimental measurements where a large background from QCD multijet processes becomes necessary to be rejected, whereas the W boson process-dependent decay channel was already algorithmically set up in this computation.

4. Phenomenological results

The differential production cross sections for the W+jets process were calculated as a function of the jet multiplicity N_{jets} in the fiducial phase-space. The differential cross sections were calculated up to one jet at NLO in Table 1 and up to two jets at NNLO in Table 2. The differential results in different regions of the $m_T(W)$ variable of the W boson are given in Table 3. The maximum and minimum scale uncertainties are also included in percent to the central results. The W^+ boson decay channel has higher differential cross sections in comparison to the W^- boson decay channel evaluated either at NLO or NNLO. The uncertainties in the differential cross sections were significantly reduced at NNLO. The uncertainties were down at $\sim$2% level for the one associated jet production case at NNLO. The comparison of uncertainties for $m_T(W)$ depends on a particular range, but overall the precision increases in the NNLO differential results with respect to the NLO ones.

Table 1. The differential cross sections as a function of N_{jets} for the $W^+ + X \to e^+\nu_e + X$ and $W^- + X \to e^-\bar{\nu}_e + X$ processes calculated up to one jet at NLO. The scale uncertainties due to the variations in μ_R and μ_F are quoted in percent in addition to the central values.

N_{jets}	$d\sigma_{NLO}/dN_{jets}$ $(W^+ + X \to e^+\nu_e + X)$	$d\sigma_{NLO}/dN_{jets}$ $(W^- + X \to e^-\bar{\nu}_e + X)$
1	$561.31^{+11.97\%}_{-9.62\%}$ pb	$458.73^{+11.97\%}_{-9.62\%}$ pb

Table 2. The differential cross sections as a function of N_{jets} for the $W^+ + X \to e^+\nu_e + X$ and $W^- + X \to e^-\bar{\nu}_e + X$ processes calculated up to two jets at NNLO. The scale uncertainties due to the variations in μ_R and μ_F are quoted in percent in addition to the central values.

N_{jets}	$d\sigma_{NNLO}/dN_{jets}$ $(W^+ + X \to e^+\nu_e + X)$	$d\sigma_{NNLO}/dN_{jets}$ $(W^- + X \to e^-\bar{\nu}_e + X)$
1	$622.80^{+1.95\%}_{-2.83\%}$ pb	$497.11^{+1.99\%}_{-2.40\%}$ pb
2	$194.79^{+25.45\%}_{-18.34\%}$ pb	$154.06^{+25.45\%}_{-18.34\%}$ pb

Table 3. The differential cross sections in bins of $m_T(W)$ for the $W^+ + X \to e^+\nu_e + X$ and $W^- + X \to e^-\bar{\nu}_e + X$ processes calculated at NLO and NNLO. The results are presented for the $m_T(W)$ ranges in 0–1000 GeV. The scale uncertainties due to the variations in μ_R and μ_F are quoted in percent in addition to the central values.

$m_T(W)$ (GeV)	$d\sigma_{NLO}/dm_T(W)$ $W^+ + X \to e^+\nu_e + X$	$d\sigma_{NLO}/dm_T(W)$ $W^- + X \to e^-\bar{\nu}_e + X$	$d\sigma_{NNLO}/dm_T(W)$ $W^+ + X \to e^+\nu_e + X$	$d\sigma_{NNLO}/dm_T(W)$ $W^- + X \to e^-\bar{\nu}_e + X$
0–15	$0.13^{+11.97\%}_{-9.62\%}$ pb	$0.07^{+11.97\%}_{-10.00\%}$ pb	$0.37^{+20.75\%}_{-15.29\%}$ pb	$0.17^{+10.87\%}_{-8.86\%}$ pb
15–20	$0.84^{+11.97\%}_{-9.62\%}$ pb	$0.27^{+11.97\%}_{-9.62\%}$ pb	$1.45^{+12.95\%}_{-10.23\%}$ pb	$0.70^{+5.44\%}_{-5.36\%}$ pb
20–30	$2.85^{+11.97\%}_{-9.62\%}$ pb	$2.59^{+11.97\%}_{-9.62\%}$ pb	$5.31^{+15.05\%}_{-11.59\%}$ pb	$4.74^{+13.90\%}_{-10.84\%}$ pb
30–40	$9.45^{+11.97\%}_{-9.62\%}$ pb	$6.03^{+11.97\%}_{-9.62\%}$ pb	$14.80^{+8.54\%}_{-6.87\%}$ pb	$9.79^{+8.23\%}_{-7.16\%}$ pb
40–60	$732.04^{+4.44\%}_{-6.52\%}$ pb	$571.24^{+4.23\%}_{-5.33\%}$ pb	$672.53^{+3.40\%}_{-3.67\%}$ pb	$643.80^{+1.37\%}_{-2.44\%}$ pb
60–100	$115751.00^{+2.91\%}_{-5.02\%}$ pb	$88541.02^{+3.01\%}_{-5.18\%}$ pb	$118795.92^{+0.91\%}_{-0.90\%}$ pb	$91113.38^{+0.85\%}_{-1.04\%}$ pb
100–1000	$76.16^{+2.81\%}_{-4.29\%}$ pb	$50.38^{+3.01\%}_{-4.58\%}$ pb	$82.64^{+1.86\%}_{-2.43\%}$ pb	$58.60^{+2.01\%}_{-2.53\%}$ pb

The differential cross section distributions for the W+jets process were calculated as functions of the $p_T(W)$, $p_T(e)$, and $p_T(j_1)$ in the fiducial phase-space. The p_T is an important variable having more sensitivity to higher-order corrections in cross section calculations. The p_T distributions were calculated at NLO and NNLO and were overlaid in the same plot for comparisons. The differential distributions for the $p_T(W)$, $p_T(e)$, and $p_T(j_1)$ are given in Figures 1–3, respectively. In the $p_T(j_1)$ distributions, p_T of the first leading jet (the hardest jet ordered in p_T) are plotted. Moreover, the differential cross sections were calculated as functions of the leading jet absolute rapidity $|y(j_1)|$ and the electron (antielectron) absolute pseudorapidty $|\eta(e^{\pm})|$ to cover variables used in the fiducial phase-space definition in addition to p_T variable. The $|y(j_1)|$ and $|\eta(e^{\pm})|$ distributions were calculated at NLO and NNLO and were overlaid in the same plot for comparisons as shown in Figures 4 and 5, respectively. The differential distributions in each plot are given for the W^+ and W^- boson decay channels separately to be able to better compare NLO and NNLO results in those channels. The systematic uncertainties due to the variations in μ_R and μ_F scales are shown in hatched bands around central points in each differential distribution.

The shapes of the differential distributions were overall consistent at NLO and NNLO for the p_T variables, while the NNLO calculation predicted slightly higher differential cross sections for the higher ranges of the p_T variables. In the $p_T(W)$ differential distributions, any peak not present in the low-$p_T(W)$ region as nonperturbative effects from soft-gluon radiation in these (N)NLO perturbative calculations were not accounted for. The difference in the differential shapes for the higher ranges of the $p_T(j_1)$ variable at NLO and NNLO can be due to different subtraction methods used in the calculations. The $p_T(e)$ and $p_T(j_1)$ differential distribution shapes were almost comparable; however, the $p_T(e)$ spectrum was lower than $p_T(j_1)$ spectrum implying that

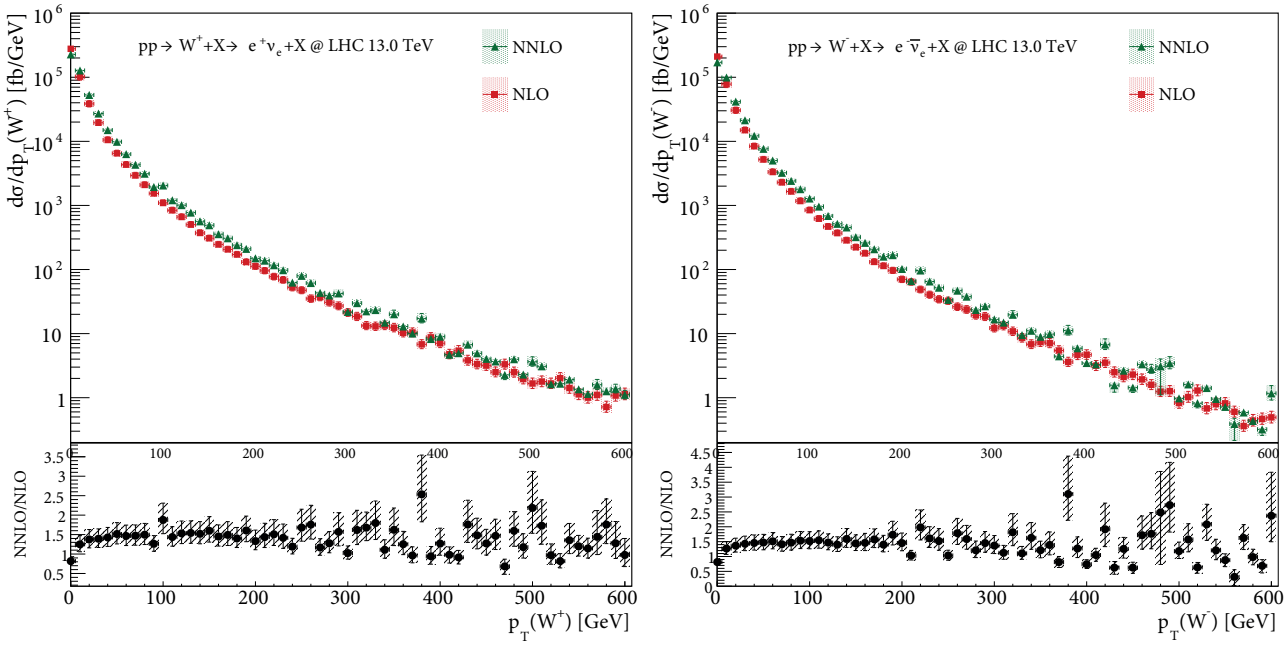

Figure 1. The differential cross sections as a function of the $p_T(W^{\pm})$ for the $W^+ + X \to e^+\nu_e + X$ (left) and $W^- + X \to e^-\bar{\nu}_e + X$ (right) processes calculated at NLO and NNLO. The results are presented for the $p_T(W^{\pm})$ ranges in 0–600 GeV. The scale uncertainties due to the variations in μ_R and μ_F are included in colored hatched bands around central points. In the lower panels, differential cross section ratios of $\mathrm{d}\sigma_{NNLO}/\mathrm{d}\sigma_{NLO}$ are included with upper and lower uncertainties due to variations of corresponding cross sections by scale uncertainties.

the jets were more energetic in particular at higher p_T ranges. The NNLO calculation predicted slightly higher differential cross section for the $|y(j_1)|$ variable while preserving the same shape with the NLO calculation. The NLO and NNLO calculations were in good agreement for the $|\eta(e^{\pm})|$ variable, both in distribution shape and central results. The differential distributions were consistent in shape for all the variables considered in the W^+ and W^- boson decay modes. In all of the differential distributions, the NNLO calculations give precise results in almost all the ranges that are higher than or comparable to the NLO results. However, there are a few exceptions such as the higher ranges of the p_T variables where the NNLO calculations can be further improved to control the fluctuations in the respective uncertainties.

The total integrated cross section results were derived for the fiducial phase-space of the W+jets process. The total cross sections were calculated at LO, NLO, and NNLO for both the W^+ and W^- boson decay channels for comprehensive comparisons. Two results are reported at NNLO based on the r_{cut} by means of the q_T-subtraction method as discussed in Section 2. The NNLO cross sections were calculated by using a fixed cut-off value of $r_{cut} = 0.15\%$ ($\sigma_{NNLO}^{r_{cut}}$) and by using the extrapolation in the limit $r_{cut} \to 0$ ($\sigma_{NNLO}^{extrapolated}$). The $r_{cut} \to 0$ extrapolation of the cross section was obtained by the MATRIX framework using a quadratic least χ^2 fit in the r_{cut} interval of 0.15%–1.0% [11]. Total rates were calculated with corresponding scale uncertainties for the LO, NLO, and NNLO predictions. Table 4 summarizes the total cross sections calculated at LO, NLO, and NNLO in the fiducial phase-space for both $W^+ + X \to e^+\nu_e + X$ and $W^- + X \to e^-\bar{\nu}_e + X$ processes. Besides, the relatives sizes of the radiative corrections in terms of K factors at NLO and NNLO were calculated as $K_{NLO} = \sigma_{NLO}/\sigma_{LO}$ and $K_{NNLO} = \sigma_{NNLO}/\sigma_{NLO}$. The K factors, showing the sizes of the included higher-order corrections in the cross section calculations at NLO and NNLO, are reported in Table 5.

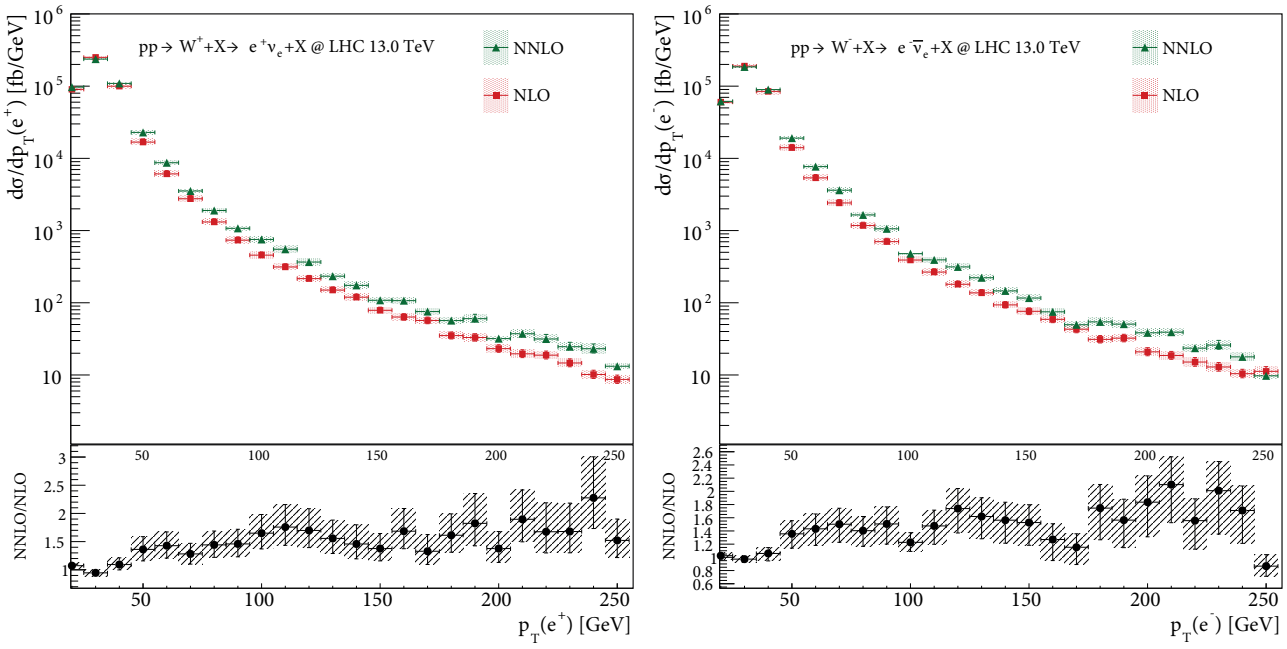

Figure 2. The differential cross sections as a function of the $p_T(e^{\pm})$ for the $W^+ + X \to e^+\nu_e + X$ (left) and $W^- + X \to e^-\bar{\nu}_e + X$ (right) processes calculated at NLO and NNLO. The results are presented for the $p_T(e^{\pm})$ ranges in 0–250 GeV. The scale uncertainties due to the variations in μ_R and μ_F are included in colored hatched bands around central points. In the lower panels, differential cross section ratios of $\mathrm{d}\sigma_{NNLO}/\mathrm{d}\sigma_{NLO}$ are included with upper and lower uncertainties due to variations of corresponding cross sections by scale uncertainties.

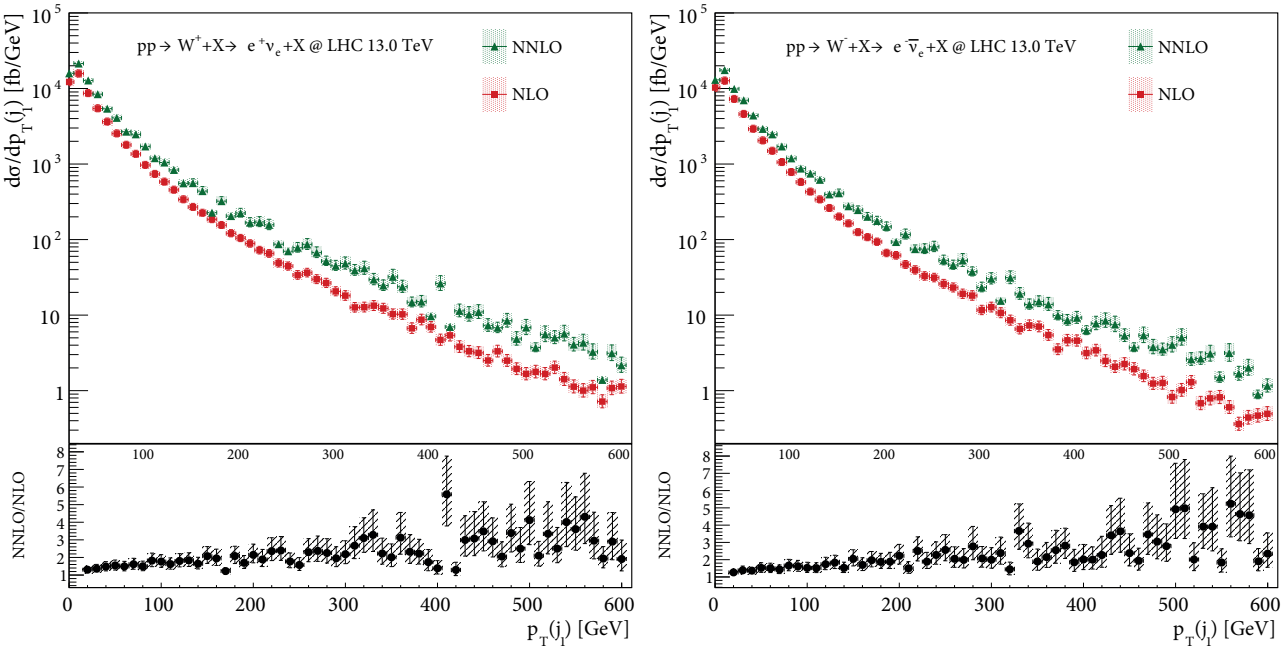

Figure 3. The differential cross sections as a function of the $p_T(j_1)$ for the $W^+ + X \to e^+\nu_e + X$ (left) and $W^- + X \to e^-\bar{\nu}_e + X$ (right) processes calculated at NLO and NNLO. The results are presented for the $p_T(j_1)$ ranges in 0–600 GeV. The scale uncertainties due to the variations in μ_R and μ_F are included in colored hatched bands around central points. In the lower panels, differential cross section ratios of $\mathrm{d}\sigma_{NNLO}/\mathrm{d}\sigma_{NLO}$ are included with upper and lower uncertainties due to variations of corresponding cross sections by scale uncertainties.

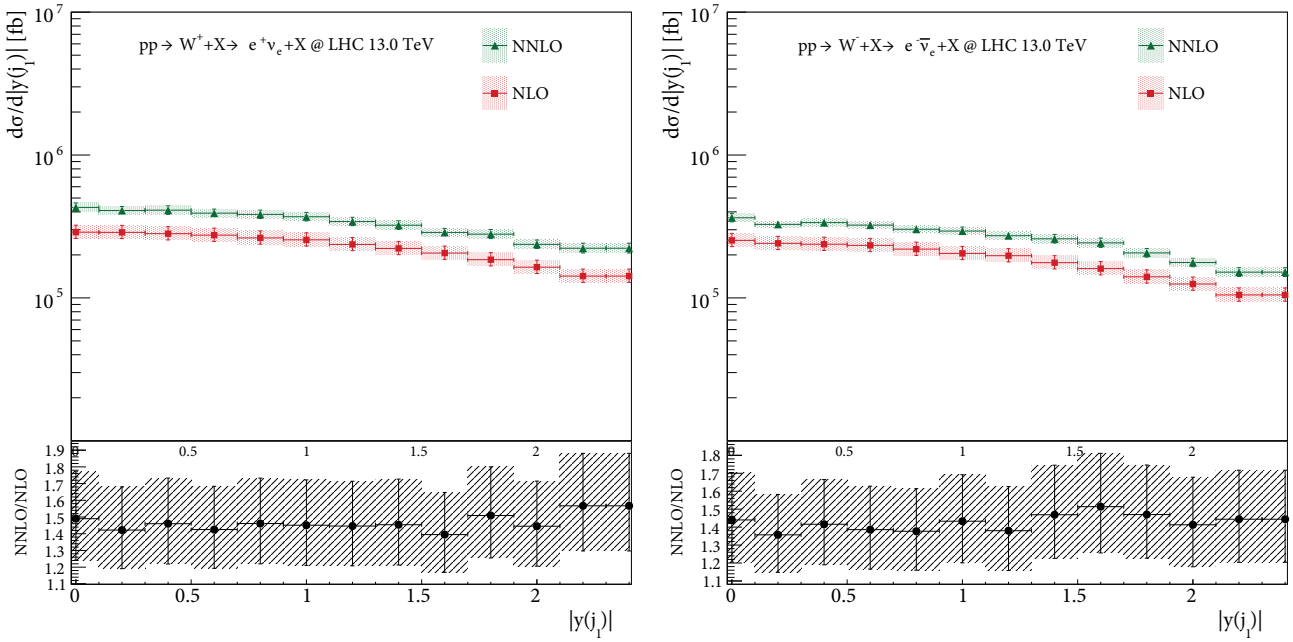

Figure 4. The differential cross sections as a function of the $|y(j_1)|$ for the $W^+ + X \to e^+\nu_e + X$ (left) and $W^- + X \to e^-\bar{\nu}_e + X$ (right) processes calculated at NLO and NNLO. The results are presented for the $|y(j_1)|$ ranges in 0–2.4. The scale uncertainties due to the variations in μ_R and μ_F are included in colored hatched bands around central points. In the lower panels, differential cross section ratios of $\mathrm{d}\sigma_{NNLO}/\mathrm{d}\sigma_{NLO}$ are included with upper and lower uncertainties due to variations of corresponding cross sections by scale uncertainties.

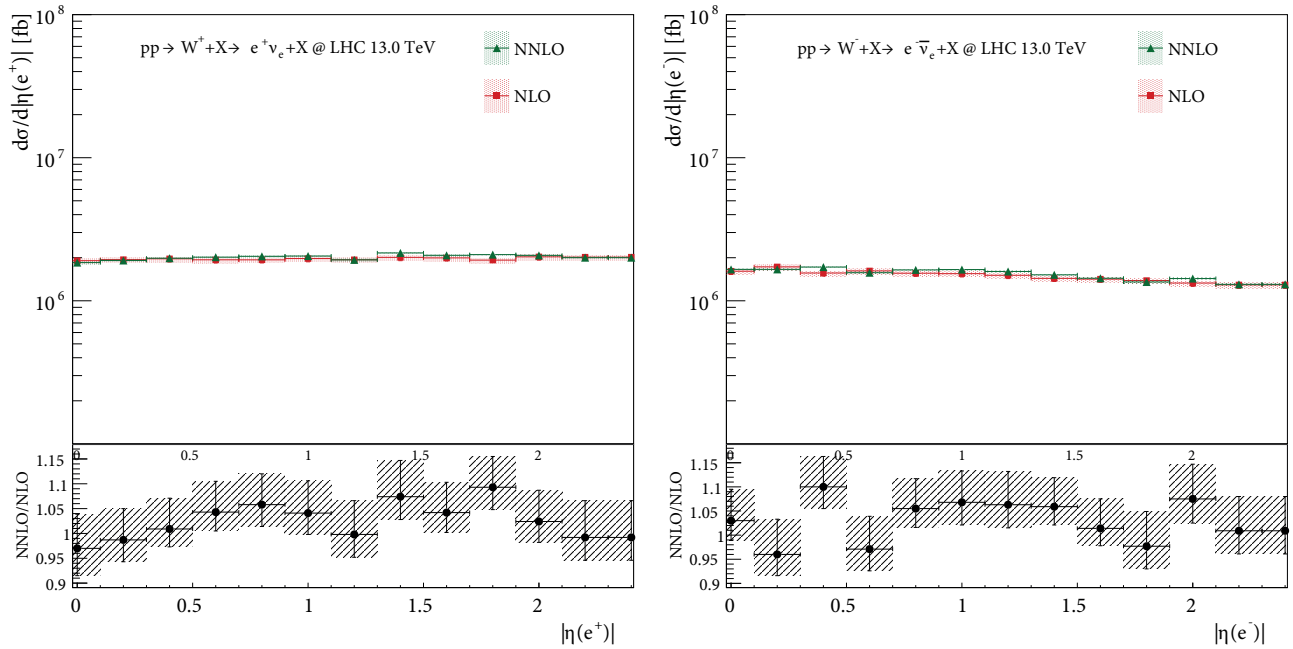

Figure 5. The differential cross sections as a function of the $|\eta(e^{\pm})|$ for the $W^+ + X \to e^+\nu_e + X$ (left) and $W^- + X \to e^-\bar{\nu}_e + X$ (right) processes calculated at NLO and NNLO. The results are presented for the $|\eta(e^{\pm})|$ ranges in 0–2.4. The scale uncertainties due to the variations in μ_R and μ_F are included in colored hatched bands around central points. In the lower panels, differential cross section ratios of $\mathrm{d}\sigma_{NNLO}/\mathrm{d}\sigma_{NLO}$ are included with upper and lower uncertainties due to variations of corresponding cross sections by scale uncertainties.

The results at different accuracies in Table 4 show that W^- boson is less produced than W^+ boson in pp collisions. The ratio of the cross sections is $\sigma_{W^-}/\sigma_{W^+} \simeq 0.76$, which is essentially independent of the perturbative order of the calculated cross sections. The difference in the production rates points to a strong asymmetry in the electron decay channels of the W boson. In addition to this interpretation, the best cross section at NNLO was obtained when using the calculation in the extrapolation of $r_{cut} \to 0$ in the q_T-subtraction formalism. The total rates were predicted to be higher in $\sigma_{NNLO}^{extrapolated}$ results than $\sigma_{NNLO}^{r_{cut}}$ ones implying that QCD corrections at NNLO were better handled using the $r_{cut} \to 0$ extrapolation approach. Table 5 supports this observation as the $K_{NNLO}^{extrapolated}$ values were significantly higher than $K_{NNLO}^{r_{cut}}$ values. The precision of the total cross section results was improved from LO results towards NLO and NNLO calculations. The uncertainties due to the scale variations were at 14% level at LO and were reduced to $\sim$5% at NLO and $\sim$1% at NNLO.

Table 4. The total production cross sections in the fiducial phase-space for the $W^+ + X \to e^+\nu_e + X$ and $W^- + X \to e^-\bar{\nu}_e + X$ processes calculated at LO, NLO, and NNLO. The NNLO cross sections are reported for a fixed cut-off value of $r_{cut} = 0.15\%$ ($\sigma_{NNLO}^{r_{cut}}$) and for the extrapolation in the limit $r_{cut} \to 0$ ($\sigma_{NNLO}^{extrapolated}$). The scale uncertainties due to the variations in μ_R and μ_F are associated to the central results in percent.

Process	σ_{LO}	σ_{NLO}	$\sigma_{NNLO}^{r_{cut}}$	$\sigma_{NNLO}^{extrapolated}$
$W^+ + X \to e^+\nu_e + X$	$3848^{+13.8\%}_{-14.4\%}$ pb	$4710^{+2.9\%}_{-5.0\%}$ pb	$4840^{+0.9\%}_{-0.9\%}$ pb	$4970^{+0.6\%}_{-1.1\%}$ pb
$W^- + X \to e^-\bar{\nu}_e + X$	$2910^{+14.2\%}_{-14.9\%}$ pb	$3600^{+3.0\%}_{-5.2\%}$ pb	$3710^{+0.8\%}_{-1.1\%}$ pb	$3802^{+0.5\%}_{-1.2\%}$ pb

Table 5. The relative sizes of the higher-order corrections in the total NLO and NNLO cross sections by means of the K factors in the $W^+ + X \to e^+\nu_e + X$ and $W^- + X \to e^-\bar{\nu}_e + X$ decay channels. The K factors for the representation of the correction sizes at NNLO were calculated separately using the$\sigma_{NNLO}^{r_{cut}}$ and $\sigma_{NNLO}^{extrapolated}$ results.

Process	K_{NLO}	$K_{NNLO}^{r_{cut}}$	$K_{NNLO}^{extrapolated}$
$W^+ + X \to e^+\nu_e + X$	+22.5%	+2.7%	+5.4%
$W^- + X \to e^-\bar{\nu}_e + X$	+23.8%	+3.1%	+5.6%

5. Conclusion

In this paper, the differential cross sections and the total cross sections are presented in the fiducial phase-space of the W boson production in association with jets in pp collisions at a center-of-mass-energy of 13 TeV. The cross sections were calculated for $W^+ + X \to e^+\nu_e + X$ and $W^- + X \to e^-\bar{\nu}_e + X$ decay modes at the perturbative orders of NLO and NNLO. The MATRIX computational framework was used to perform calculations by applying realistic fiducial cuts for the decay products of the W boson. The Catani–Seymour dipole subtraction method was used in the NLO computation. On the other hand, the q_T-subtraction method was used for the evaluation of the IR divergences in the NNLO computation. The NNLO differential cross sections were obtained using a fixed residual dependence parameter cut $r_{cut} = 0.15\%$ in the q_T-subtraction formalism. The total production cross sections at NNLO were calculated using both $r_{cut} = 0.15\%$ and the extrapolation in the limit $r_{cut} \to 0$. In the entire calculation procedure, systematic uncertainties due the variations in the μ_R and μ_F scales are included for the estimation of the perturbative uncertainties at each order. The *NNPDF30* PDF sets are used in the cross section calculations that are based on constant strong coupling $\alpha_s(m_Z) = 0.118$.

The differential cross sections were calculated as functions of the jet multiplicity N_{jets} up to one (two) jet(s) at (N)NLO and of the invariant mass of the W boson $m_T(W)$. The corresponding uncertainties were significantly reduced for the N_{jets} and $m_T(W)$ variables in the NNLO results. The differential results were also obtained for the transverse momenta of the W boson $p_T(W)$, the electron $p_T(e)$, and the leading jet $p_T(j_1)$ that were compared at NLO and NNLO. The results were consistent in both distribution shapes and central values at NLO and NNLO, while the NNLO calculation predicts higher cross sections in the higher ranges of the p_T variables. The accuracy of the NNLO calculations were generally comparable or higher in comparison to NLO results. Exceptionally, the fluctuations in the uncertainties of the NNLO calculations in the higher ranges of the p_T variables can be reduced to further improve the level of precision. The differential cross sections were also calculated for the absolute rapidity of the leading jet $|y(j_1)|$ and the absolute pseudorapidity of the electron $|\eta(e^{\pm})|$. The NLO and the NNLO distribution shapes were consistent for the $|y(j_1)|$ and $|\eta(e^{\pm})|$ variables, where the NNLO calculation tended to predict higher differential cross sections for the $|y(j_1)|$ variable. The differential cross sections at NLO and NNLO were almost the same over the entire ranges of the $|\eta(e^{\pm})|$ variable; thus, this variable among others appears to be less sensitive to the inclusion of the NNLO corrections. In all of the differential results, the predicted cross sections were higher in the W^+ boson decay channel than the corresponding ones in the W^- boson decay channel. The differential cross section results in this paper show that NNLO calculation is crucial for the precise description of the W+jets production differentially as functions of the important variables.

The total production cross sections were also calculated and compared at the LO, NLO, and NNLO accuracies in the W^+ and W^- boson decay channels separately. The total cross sections were higher at NNLO than the corresponding ones calculated at LO and NLO. The total cross sections were higher in the extrapolation of $r_{cut} \to 0$ limit than the ones obtained using the fixed cut-off $r_{cut} = 0.15\%$ in the q_T-subtraction formalism at NNLO. The relatives sizes of the QCD radiative corrections in terms of K factors were calculated. The K factor was higher in the $r_{cut} \to 0$ extrapolation limit than that calculated for the fixed $r_{cut} = 0.15\%$ at NNLO; therefore, the best NNLO results were obtained in the extrapolation approach in terms of the inclusion of more QCD corrections. The included higher-order corrections in the total rates were up to 5.6% at NNLO, while the NLO corrections were as large as 23.8%. Furthermore, the calculated total rates show that W^- boson is less produced than W^+ boson in pp collisions. The ratios of the production rates were $\sigma_{W^-}/\sigma_{W^+} \simeq 0.76$ regardless of the perturbative order at which the calculation was performed. The K factors in the calculations turned out to be slightly higher in the decay of W^- boson than the corresponding ones in the W^+ boson decay channel. Moreover, the precision of the total cross sections was improved significantly from LO results towards the NLO and NNLO calculations. The uncertainties due to the scale variations were at 14% level at LO and are reduced to $\sim$5% at NLO and $\sim$1% at NNLO.

Finally, the predicted differential and total cross section calculations can be used in comparisons with experimental data. In particular, the NNLO calculations employing the q_T-subtraction approach can be used for accurate description of data from the LHC experiments. The NNLO differential calculations performed in the fiducial phase-space of the W+jets production are already satisfying in terms of the precision achieved. The NNLO differential calculations can clearly be suggested for comparisons with the unfolded experimental data of the LHC experiments.

References

[1] Khachatryan, V.; Sirunyan, A. M.; Tumasyan, A.; Adam, W.; Bergauer, T.; Dragicevic, M.; Erö, J.; Fabjan, C.; Friedl, M.; Fruehwirth, R. et. al. *Phys. Lett. B* **2015**, *741*, 12-37.

[2] Khachatryan, V.; Sirunyan, A. M.; Tumasyan, A.; Adam, W.; Aşılar, E.; Bergauer, T.; Brandstetter, J.; Brondolin, E.; Dragicevic, M.; Erö, J. et. al. *Phys. Rev. D* **2017**, *95*, 052002.

[3] Aad, G.; Abbott, B.; Abdallah, J.; Khalek, S. A.; Abdinov, O.; Aben, R.; Abi, B.; Abolins, M.; AbouZeid, O.; Abramowicz, H. et al. *Eur. Phys. J. C* **2015**, *75*, 82.

[4] Aaboud, M.; Aad, G.; Abbott, B.; Abdinov, O.; Abeloos, B.; Abidi, S. H.; AbouZeid, O.; Abraham, N.; Abramowicz, H.; Abreu, H. et al. *J. High Energy Phys.* **2018**, *05*, 077.

[5] Aaij, R.; Beteta, C. A.; Adeva, B.; Adinolfi, M.; Ajaltouni, Z.; Akar, S.; Albrecht, J.; Alessio, F.; Alexander, M.; Ali, S. et al. *J. High Energy Phys.* **2016**, *05*, 131.

[6] Sirunyan, A. M.; Tumasyan, A.; Adam, W.; Ambrogi, F.; Aşılar, E.; Bergauer, T.; Brandstetter, J.; Brondolin, E.; Dragicevic, M.; Erö, J. et. al. *Phys. Rev. D* **2017**, *96*, 072005.

[7] Aaboud, M.; Aad, G.; Abbott, B.; Abdallah, J.; Abdinov, O.; Abeloos, B.; Aben, R.; AbouZeid, O.; Abraham, N.; Abramowicz, H. et al. *Phys. Lett. B* **2017**, *765*, 132-153.

[8] Boughezal, R.; Campbell, J. M.; Ellis, R. K.; Focke, C.; Giele, W. T.; Liu, X.; Petriello, F. *Phys. Rev. Lett.* **2016**, *116*, 152001.

[9] Boughezal, R.; Liu, X.; Petriello, F. *Phys. Rev. D* **2016**, *94*, 113009.

[10] Boughezal, R.; Focke, C.; Liu, X.; Petriello, F. *Phys. Rev. Lett.* **2015**, *115*, 062002.

[11] Grazzini, M.; Kallweit, S.; Wiesemann, M. *Eur. Phys. J. C* **2018**, *78*, 537.

[12] Catani, S.; Cieri, L.; Ferrera, G.; de Florian, D.; Grazzini, M. *Phys. Rev. Lett.* **2009**, *103*, 082001.

[13] Catani, S.; Grazzini, M. *Phys. Rev. Lett.* **2007**, *98*, 222002.

[14] Catani, S.; Cieri, L.; de Florian, D.; Ferrera, G.; Grazzini, M. *Eur. Phys. J. C* **2012**, *72*, 2195.

[15] Catani, S.; Seymour, M. H. *Phys. Lett. B* **1996**, *378*, 287-301.

[16] Catani, S.; Seymour, M. H. *Nucl. Phys. B* **1997**, *485*, 291-419.

[17] Cascioli, F.; Maierhofer, P.; Pozzorini, S. *Phys. Rev. Lett.* **2012**, *108*, 111601.

[18] Buccioni, F.; Pozzorini, S.; Zoller, M. *Eur. Phys. J. C* **2018**, *78*, 70.

[19] Matsuura, T.; van der Marck, S. C.; van Neerven, W. L. *Nucl. Phys. B* **1989**, *319*, 570-622.

[20] Denner, A.; Dittmaier, S.; Hofer, L. *Commun. Comput. Phys.* **2017**, *212*, 220-238.

[21] Catani, S.; Cieri, L.; de Florian, D.; Ferrera, G.; Grazzini, M. *Nucl. Phys. B* **2014**, *881*, 414-443.

[22] Buckly, A.; Ferrando, J.; Lloyd, S.; and Nordström, K.; Page, B.; Rüfenacht, M.; Schönherr, M.; Watt, G. *Eur. Phys. J. C* **2015**, *75*, 132.

[23] Ball, R. D.; Bertone, V.; Carrazza, S.; Deans, C. S.; Debbio, L. D.; Forte, S.; Guffanti, A.; Hartland, N. P.; Latorre, J. I.; Rojo, J. et al. *J. High Energy Phys.* **2015**, *04*, 040.

[24] Cacciari, M.; Salam, G. P.; Soyez, G. *J. High Energy Phys.* **2008**, *04*, 063.